Effect of decoupled azimuthal and zenithal anchoring on smectic-*C* chevron structures

Alberto Diaz, Geoff McKay, and Nigel J. Mottram
Department of Mathematics, University of Strathclyde, 26 Richmond Street, Glasgow G1 1XH, United Kingdom
(Received 9 May 2007; published 24 October 2007)

We present a study of the effect of decoupled azimuthal and zenithal weak anchoring on the transition between C1 and C2 chevron structures in smectic-*C* liquid crystals. We consider temperatures below the Sm*A*-Sm*C* transition and assume that the value of the smectic cone angle can be regarded as constant through the cell. By standard Euler-Lagrange minimization of the total energy we obtain a simple analytical expression for the equilibrium director twist angle in the C1 and C2 chevron states. Using this analytical form, we are able to compare the total energies of the C1 and C2 chevrons, and determine the globally stable chevron profile. We show that the C2 state is preferred when the azimuthal anchoring strength is relatively large, while C1 chevrons will dominate for strong zenithal anchoring.

DOI: 10.1103/PhysRevE.76.041705 PACS number(s): 61.30.Dk, 61.30.Hn

I. INTRODUCTION

Layered chevron structures can appear when a confined sample of smectic-*A* liquid crystal is cooled into the tilted smectic-*C* phase. In a constrained system where layer continuity is conserved, the molecular tilting associated with this change of phase, and the corresponding layer thickness contraction, can lead to layer buckling. When this type of buckling occurs the smectic layers can orientate in one of two directions, leading to what are known as C1 or C2 chevrons. As a result of this degeneracy in the layer direction, the liquid crystal can organize into domains of different chevron states. However, the interfaces between these domains form "zigzag" defects [1,2], which can have a detrimental effect on the quality of liquid crystal displays.

In order to exploit the display possibilities of surface stabilized ferroelectric liquid crystals (SSFLCs), it is vital to have an understanding of and some control over the self-organization of confined smectic layers. One way of breaking the smectic layer degeneracy, thereby predisposing the system toward one of the C1 or C2 states, is to treat the bounding substrates so that a specified director angle (a "pretilt") is induced at the surfaces. Introducing this type of tilt anchoring can lead to the removal of defects and a homogeneous device with better optical characteristics.

A number of theoretical models have been proposed for smectic chevron structures. Clark and Rieker [2] presented the first theoretical description, modeling chevrons in terms of a discontinuity in layer tilt while maintaining a continuous director structure at the chevron interface. Nakagawa [3,4], Mukai and Nakagawa [5], and Anderson [6] considered compressible (variable thickness) smectics, while de Meyere *et al.* [7] adopted a similar approach that assumed the molecule tilt was related to the layer tilt. Limat and Prost [8] examined the transition between the smectic-*A* bookshelf structure and the smectic-*C* chevron, while Limat [9] extended Nakagawa's model [4] to allow for unequal cone and layer tilt angles. Mottram *et al.* [10] assumed that the layer and molecule tilts were related in their study of biaxiality in the smectic-*C* phase. Phenomenological Landau–de Gennes free energy functionals similar to [10] were also employed in studies of smectics by Vaupotič *et al.* [11], Beldon *et al.* [12], and Shalaginov *et al.* [13,14].

The present authors have previously examined the transition between C1 and C2 chevron profiles close to the Sm*A*–Sm*C* transition and, by adopting a simplified elastic energy density and a low-order thermodynamic Landau expansion, were able to derive, analytically, phase diagrams demarcating the C1 and C2 regimes for variable temperature, pretilt, and anchoring strength. It was found that the C2 state is preferred when the pretilt angle is decreased and/or the anchoring strength is weakened. This behavior was confirmed by Diaz *et al.* [15,16] via a numerical model of the weak pretilt anchoring.

However, the results of [15,16] appear to contradict a related analysis by Wang *et al.* [17], who found that, for their choice of surface energy, C1 chevrons are preferred at weak anchoring strengths. Upon closer inspection it is clear that the surface energy adopted in Wang *et al.* [17] is a measure of only the azimuthal variation from the preferred director position at the substrate. The apparent contradiction may be due to the models of Wang *et al.* and Diaz *et al.* considering only restricted versions of the surface anchoring energy.

In an attempt to isolate the mechanisms that determine the existence of C1 or C2 chevrons, in this article we examine the effect of decoupled azimuthal and zenithal surface energies. Unlike previous studies [15,16], we consider chevrons at a temperature below the Sm*A*–Sm*C* transition where the cone angle and chevron tilt angle are assumed to be fixed. We could introduce variations in the cone angle via a thermodynamic Landau expansion similar to [15,16] but our aim here is to concentrate on the influence of azimuthal and zenithal anchoring and this energy term is omitted. From geometry considerations, we will show that the surface energy adopted in Diaz *et al.* [15,16] can be thought of as a special case of a general energy form in which the individual azimuthal and zenithal anchoring strength coefficients are equal.

By standard Euler-Lagrange minimization of the total energy, we obtain a simple analytical expression for the equilibrium director twist angle in the C1 and C2 chevron states. This in turn allows us to compare the total energies of the C1 and C2 chevrons and determine the globally stable chevron profile. We examine the equilibrium director profiles and chevron structures that minimize the energy as the azimuthal and zenithal anchoring strength coefficients are allowed to vary independently.

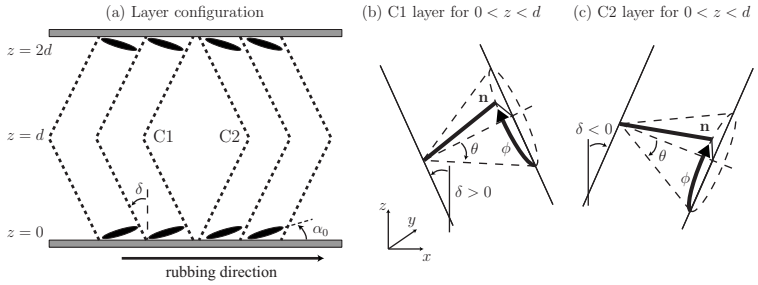

FIG. 1. (a) Layer configuration for C1 and C2 chevron structures; (b), (c) Description of the director in the region $0<z<d$ for, respectively, C1 and C2 layers, illustrating the cone angle θ, azimuthal angle ϕ, and layer tilt angle δ.

II. GEOMETRY OF THE CELL

We examine a smectic-*C* liquid crystal sample constrained by two parallel substrates a distance $2d$ apart [see Fig. 1(a)]. The z axis corresponds to the direction perpendicular to the substrates, the x axis coincides with the rubbing direction on the substrates, while the y axis completes the orthogonal coordinate system. We consider symmetric substrate treatments (often called *parallel* rubbing); therefore, we model the lower half of the cell, from $z=0$ to $z=d$, and assume that the upper half is equivalent due to symmetry. Nonsymmetric configurations may exist [18]; however, they will be energetically unfavorable.

The smectic-*C* phase can be described as a layered structure where the unit director $\mathbf{n}$ makes an angle θ (>0), the cone angle, with respect to the layer normal. The director is then constrained to lie on the surface of a fictitious cone, with vertex angle 2θ; see Figs. 1(b) and 1(c). The position of $\mathbf{n}$ on this smectic-*C* cone can be represented via an azimuthal angle ϕ, while the layer tilt angle δ denotes the tilt of the layers from the substrate normal. The cone angle is dependent on temperature [19] and, although influences such as an applied electric field or surface treatments may alter the cone angle from the thermotropic equilibrium, we will assume that the cone angle is constant through the cell. Furthermore, in this model we will also assume an empirically derived relationship between the layer tilt, which is largely determined by the steric packing of molecules in layers, and the cone angle, defined by the local optic axis which is determined by the orientation of the molecular core. This relationship between the layer tilt and cone angle will be taken as $\delta = \pm \mu\theta$, where $\mu=0.85$ is a typical experimentally determined value [20,21]. The C1 and C2 chevrons are then characterized by, respectively, a positive or negative layer tilt angle δ in the lower half of the cell; see Fig. 1(a). Assuming that the twist angle, $\phi(z)$, depends on only the z coordinate, we can write the director $\mathbf{n}$ as

$$\mathbf{n} = [\cos\theta\cos\delta + \sin\theta\sin\delta\cos\phi(z), \\ -\sin\theta\sin\phi(z), \cos\theta\sin\delta - \sin\theta\cos\delta\cos\phi(z)]. \quad (1)$$

At both the substrate and the chevron interface the director will be restricted by certain constraints. At the chevron interface the two arms of the chevron, tilted in opposite directions, meet and, since the director is restricted to lie on the smectic cone, there is a geometric constraint which forces the director to lie in the xy plane, as discussed in a later section. At the substrate an anchoring treatment is applied and tends to align the director in a certain direction, as discussed in the next section.

III. SURFACE ANCHORING

A number of factors can influence the anchoring of liquid crystal molecules at a substrate, such as steric and dipole-dipole interactions between molecules and the polymer alignment layer. The macroscopic anchoring energy is a representation of these effects which is used, together with bulk energy terms, to calculate the total energy of the system. This total energy will then be minimized to find the equilibrium director configuration(s) for the liquid crystal.

A commonly used anchoring energy is the Rapini-Papoular energy term,

$$W_{\text{surf}} = \frac{1}{2}\tau_0[1 - (\mathbf{n}\cdot\mathbf{n}_0)^2], \quad (2)$$

which exhibits a minimum at $\mathbf{n}=\mathbf{n}_0$, when the director aligns with a specific preferred surface orientation, $\mathbf{n}_0$. In Eq. (2), τ_0 is the anchoring strength and, assuming that the alignment rubbing is in the x direction, the preferred orientation

$$\mathbf{n}_0 = (\cos\alpha_0,\ 0,\ \sin\alpha_0) \quad (3)$$

is written in terms of a *pretilt* angle α_0. If we define ω (as shown in Fig. 2) to be the angle between $\mathbf{n}$ and $\mathbf{n}_0$ then, using Eqs. (1) and (3),

$$\cos\omega = \mathbf{n}\cdot\mathbf{n}_0 = \cos\theta\cos(\delta-\alpha_0) + \sin\theta\cos\phi\sin(\delta-\alpha_0) \quad (4)$$

and Eq. (2) may be rewritten as

$$W_{\text{surf}} = \frac{1}{2}\tau_0\sin^2\omega, \quad (5)$$

which is clearly minimized when $\omega=0$.

However, it is often possible to associate molecular anchoring effects with an anchoring of the director in either the zenithal or azimuthal directions. For instance, steric interactions between liquid crystal molecules and the polymer alignment material may be more important as the director rotates about the axis in the xz plane which is perpendicular to $\mathbf{n}_0$, called an azimuthal rotation. Dipole-dipole interactions between liquid crystal and polymer molecules may be dominant when the director rotates within the xz plane, called a zenithal rotation. In order to investigate the individual influ-

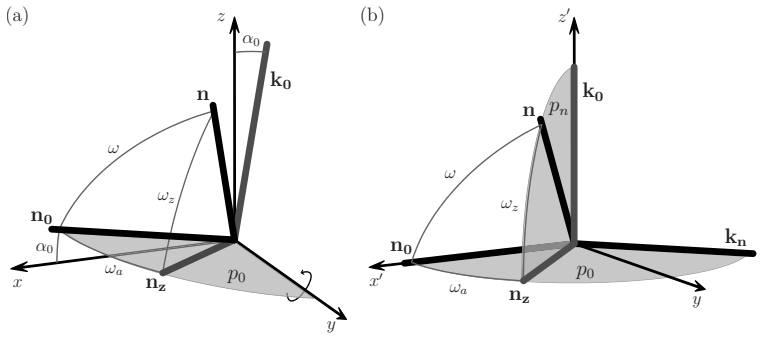

FIG. 2. (a) The director **n** and preferred surface director $\mathbf{n}_0$ at the lower surface $z=0$. (b) The same configuration as (a) following a rotation of the xz plane around the y axis through the angle α_0. Preferred surface director $\mathbf{n}_0$ now coincides with the x' axis direction and $\mathbf{k}_0$ corresponds to the z' axis direction. Zenithal angle ω_z is the tilt of director **n** with respect to p_0 within the plane p_n, while the azimuthal angle ω_a is the tilt in the plane p_0.

ences of azimuthal and zenithal anchoring, we will need to separate the anchoring energy in Eq. (2) into azimuthal and zenithal contributions.

We will use the standard definitions of the azimuthal and zenithal angles between the director **n** and the planes containing the preferred surface director $\mathbf{n}_0$. In order to determine these angles we introduce the *pretilt plane*, p_0, containing $\mathbf{n}_0$ and perpendicular to the xz plane, with normal $\mathbf{k}_0 = (-\sin\alpha_0,\ 0,\ \cos\alpha_0)$; see Fig. 2. The unit vector $\mathbf{n_z}$ is the intersection of the pretilt plane and the plane p_n, containing both $\mathbf{k}_0$ and **n**, which has unit normal $\mathbf{k_n} = \mathbf{k}_0 \times \mathbf{n}/|\mathbf{k}_0 \times \mathbf{n}|$. Since the intersection of two planes is equivalent to the vector product of their normals, the unit vector $\mathbf{n_z}$ is therefore

$$\mathbf{n_z} = \frac{\mathbf{k_n} \times \mathbf{k}_0}{|\mathbf{k_n} \times \mathbf{k}_0|} = \left(\frac{\mathbf{k}_0 \times \mathbf{n}}{|\mathbf{k}_0 \times \mathbf{n}|} \right) \times \mathbf{k}_0 \tag{6}$$

$$= \frac{\mathbf{n}(\mathbf{k}_0 \cdot \mathbf{k}_0) - \mathbf{k}_0(\mathbf{n} \cdot \mathbf{k}_0)}{\cos\omega_z} = \frac{\mathbf{n} - \mathbf{k}_0 \sin\omega_z}{\cos\omega_z}, \tag{7}$$

where the zenithal angle ω_z is the tilt of the director **n** with respect to p_0 within the plane p_n. Equation (6) uses the fact that $\mathbf{k}_0$ and $\mathbf{k_n}$ are mutually perpendicular unit vectors, while Eq. (7) recognizes that $\pi/2 - \omega_z$ is the acute angle between the unit vectors $\mathbf{k}_0$ and **n**.

The azimuthal angle ω_a between $\mathbf{n}_0$ and $\mathbf{n_z}$ in the plane p_0 can be expressed using Eq. (7) as

$$\cos\omega_a = \mathbf{n}_0 \cdot \mathbf{n_z} = \frac{\mathbf{n}_0 \cdot \mathbf{n} - \mathbf{n}_0 \cdot \mathbf{k}_0 \sin\omega_z}{\cos\omega_z} = \frac{\cos\omega}{\cos\omega_z}, \tag{8}$$

since $\mathbf{n}_0 \cdot \mathbf{n} = 0$. The surface energy (5) can now be written as

$$W_{\text{surf}} = \frac{1}{2}\tau_0(1 - \cos^2\omega_a \cos^2\omega_z)$$

$$\equiv \frac{1}{2}\tau_0(\sin^2\omega_a + \sin^2\omega_z - \sin^2\omega_a \sin^2\omega_z). \tag{9}$$

The angle ω_z can be determined in terms of α_0, θ, δ, and $\phi(z)$ via

$$\sin^2\omega_z = (\mathbf{k}_0 \cdot \mathbf{n})^2$$

$$= [\cos\theta \sin(\delta - \alpha_0) - \sin\theta \cos(\delta - \alpha_0)\cos\phi]^2. \tag{10}$$

Similarly, using Eqs. (4) and (8) it is possible to show that

$$\sin^2\omega_a = \frac{\sin^2\theta \sin^2\phi}{1 - \sin^2\omega_z}. \tag{11}$$

Our aim is to examine the preferred chevron structures when variations in zenithal and azimuthal anchoring contribute independently to the surface energy. By considering Eq. (9), an obvious way to proceed is to employ the general anchoring term,

$$W_{\text{surf}} = \frac{1}{2}(\tau_a \sin^2\omega_a + \tau_z \sin^2\omega_z - \tau_{az} \sin^2\omega_a \sin^2\omega_z), \tag{12}$$

where τ_a and τ_z are the anchoring strengths of, respectively, the azimuthal and zenithal contributions to the surface energy, and τ_{az} is a coupling coefficient. In Jérôme [22], it is shown that τ_z should vary between 10^{-3} and 10^{-7} N m^{-1}, while τ_a is between one and two orders of magnitude smaller. A physical justification for this is presented in [22], although measurements made by Vilfan [23] suggest that the azimuthal and the zenithal coefficients are of the same order.

At this point it is worth considering the possible director configurations within the cell. At the substrate the restriction of the director to lie on the smectic cone means that it is not always possible to align the director with the preferred direction $\mathbf{n}_0$. At the bottom of Fig. 3(a) we have sketched the director cone, viewed along the x axis, in both the C1 and C2 states together with the preferred orientation $\mathbf{n}_0$ at the substrate. (In this paper, we assume that α_0, the angle of $\mathbf{n}_0$ from the x axis, is positive although negative values can be considered and will result in an equivalence when C1 and C2 states are interchanged.) It is clear that the director can be aligned with the preferred orientation at the substrate in the C1 case only when $\phi(0) = \pi$ and $\alpha = \theta + \delta$. For the C2 case the director can align with the preferred direction provided $\phi(0) = \pi$ and $\alpha = \theta - \delta$. For all other values of ϕ there is a nonzero angle ω between the director and the preferred direction, so the surface energy will be nonzero. We imagine that for small pretilt angles the preferred orientation of the director (the orientation for which ω is smallest) is expected to be at $\phi(0) = 0$ in the C1 case and at $\phi(0) = \pi$ in the C2 case (although the elastic energy will also be a factor in determining the energy minimum of the total free energy). When the pretilt angle is large enough the preferred director orientations would be expected to be $\phi(0) = \pi$ in the C1 case and at $\phi(0) = \pi$ in the C2 case. At the top of Fig. 3(a) we see that

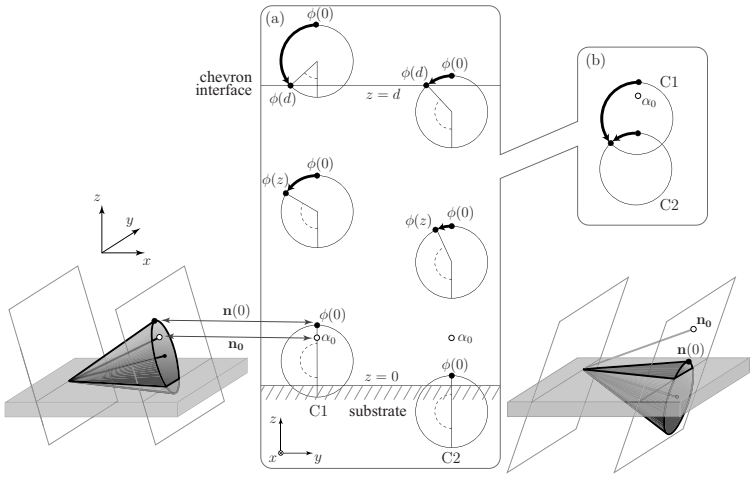

FIG. 3. Illustration of the intersection of the smectic cone in the C1 and C2 layers with the substrate. In (a) the variation of the director azimuthal angle $\phi(z)$ through the cell is shown. The azimuthal angle varies from the substrate value $\phi(0)$ to the chevron interface value $\phi(d)$, which takes the value for which the director lies in the xy plane. In (b) the representation of both the C1 and C2 director profiles is demonstrated in a single diagram.

the geometric restriction of the director orientation at the center of the cell ($z=d$) to lie in the xy plane is different in the two chevron cases. For $\delta=\mu\theta$ and $\mu<1$, $\phi(d)$ will be closer to π in the C1 case [see Eq. (17) with $\theta>\delta>0$] and closer to 0 in the C2 case [see Eq. (17) with $-\theta<\delta<0$]. In a subsequent plot we will represent the variation of ϕ through the cell, from $\phi(0)$ to $\phi(d)$, using the diagrams shown in Fig. 3(b) where we draw both the C1 and C2 cones on the same diagram and trace the path of the director on each cone as we move from the substrate to the center of the cell.

IV. ENERGY MINIMIZATION

The system will exhibit equilibrium structures that attain minimum states of the total free energy. We will consider a free energy that incorporates bulk elasticity and surface anchoring effects due to parallel rubbing. In previous analyses of chevron structures [15,16], the present authors also incorporated a thermodynamic energy density derived from a Landau expansion in the order parameter θ. However, here we examine a smectic sample at a fixed temperature far enough away from the SmA-SmC phase transition to assume that the cone angle is constant throughout the sample. The thermotropic energy may therefore be omitted.

We will use the standard Frank-Oseen nematic elastic energy density [24] within a smectic layer for the director $\mathbf{n}$ defined in Eq. (1), subject to a one elastic constant approximation,

$$W_{\text{elas}} = \frac{K_\phi}{2}\sin^2\theta\left(\frac{d\phi}{dz}\right)^2, \tag{13}$$

where K_ϕ is an elastic constant. The total energy of the system (per unit area in the xy plane) is therefore

$$\begin{aligned} E &= 2\left(\int_0^d W_{\text{elas}}\ dz + W_{\text{surf}}(0)\right) \\ &= \int_0^d K_\phi \sin^2\theta\left(\frac{d\phi}{dz}\right)^2 dz + [\tau_a \sin^2\omega_a(0) + \tau_z \sin^2\omega_z(0) \\ &\quad - \tau_{az}\sin^2\omega_a(0)\sin^2\omega_z(0)], \end{aligned} \tag{14}$$

where $\omega_z(0)$ and $\omega_a(0)$ are the expressions defined by Eqs. (10) and (11) evaluated at $z=0$, in other words, when $\phi=\phi(0)$. [The factor of 2 in Eq. (14) indicates that the energy is twice the energy of one-half of the chevron structure, between $z=0$ and $z=d$.]

The director configuration will be determined by minimization of the total energy, E. Using the standard Euler-Lagrange minimization, we obtain the bulk governing equation

$$\frac{d^2\phi}{dz^2} = 0, \tag{15}$$

and the boundary condition at $z=0$,

$$\begin{aligned} 2K_\phi \sin^2\theta\frac{d\phi}{dz} &= \frac{d}{d\phi(0)}[\tau_a \sin^2\omega_a(0) + \tau_z \sin^2\omega_z(0) \\ &\quad - \tau_{az}\sin^2\omega_a(0)\sin^2\omega_z(0)]. \end{aligned} \tag{16}$$

From geometrical considerations and the assumed symmetry of the chevron structure, the director is constrained to lie in the xy plane in the center of the cell, i.e., $\mathbf{n}_3=0$ at $z=d$. Using Eq. (1), the azimuthal angle in the center of the cell must, therefore, satisfy

$$\phi(d) = \cos^{-1}\left(\frac{\tan\delta}{\tan\theta}\right). \tag{17}$$

The minimum (and maximum) energy solutions can be found by solving Eq. (15) subject to the boundary conditions in Eq. (16) at $z=0$ and Eq. (17) at $z=d$.

The solution of Eq. (15) is a linear variation of the azimuthal angle,

$$\phi(z) = [\phi(d) - \phi(0)]\frac{z}{d} + \phi(0), \tag{18}$$

where $\phi(d)$ is given by Eq. (17) and, using Eqs. (16) and (18), $\phi(0)$ is a solution of

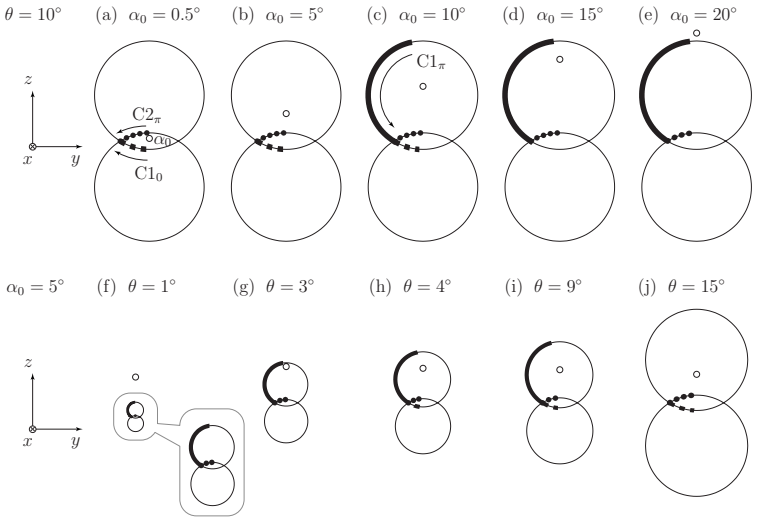

FIG. 4. The director twist angle $\phi(z)$ for C1 and C2 chevrons and the preferred director $\mathbf{n}_0$ (denoted by the small circle positioned where $\mathbf{n}_0$ intersects with the smectic layer) for variable pretilt as viewed along the x axis. In (c), (h), and (i), two stable C1 configurations coexist: $C1_0$ chevrons with ϕ_0 close to zero on the C1 cone, and $C1_\pi$ chevrons with ϕ_0 close to π radians. Dashed line, $C1_0$ chevron; solid line, $C1_\pi$ chevron; dotted line, $C2_\pi$ chevron.

$$2K_\phi \sin^2\theta \frac{[\phi(d)-\phi(0)]}{d} = \frac{d}{d\phi(0)}[\tau_a \sin^2\omega_a(0) + \tau_z \sin^2\omega_z(0) - \tau_{az}\sin^2\omega_a(0)\sin^2\omega_z(0)], \quad (19)$$

where $\omega_z(0)$ and $\omega_a(0)$ are the functions given in Eqs. (10) and (11) evaluated at $z=0$, i.e., functions of $\phi(0)$. This nonlinear equation may have more than one solution and as a result there may be more than one director configuration possible for a fixed set of parameter values. Consideration of the energy E for each configuration will determine the global energy minimizer. Using Eq. (18), we can simplify the energy in Eq. (14) to

$$E = \frac{K_\phi \sin^2\theta}{d}[\phi(d)-\phi(0)]^2 + \tau_a \sin^2\omega_a(0) + \tau_z \sin^2\omega_z(0) - \tau_{az}\sin^2\omega_a(0)\sin^2\omega_z(0). \quad (20)$$

The stability of solutions of Eq. (19) can be determined from the second derivative of the free energy, $d^2E/d\phi(0)^2$.

We will consider the solutions of Eq. (19) for both C1 and C2 chevron configurations. As mentioned previously, these two chevron structures differ in the sign of the layer tilt δ, with a C1 chevron corresponding to a layer tilt $\delta=\mu\theta$, whereas $\delta=-\mu\theta$ for a C2 chevron (we always take $\mu>0$). This difference in the value of δ affects the director angle ϕ at the chevron interface through Eq. (17), as well as the values of ω, ω_a, and ω_z through Eqs. (4), (10), and (11). Consequently, for a fixed parameter set, the C1 and C2 chev-

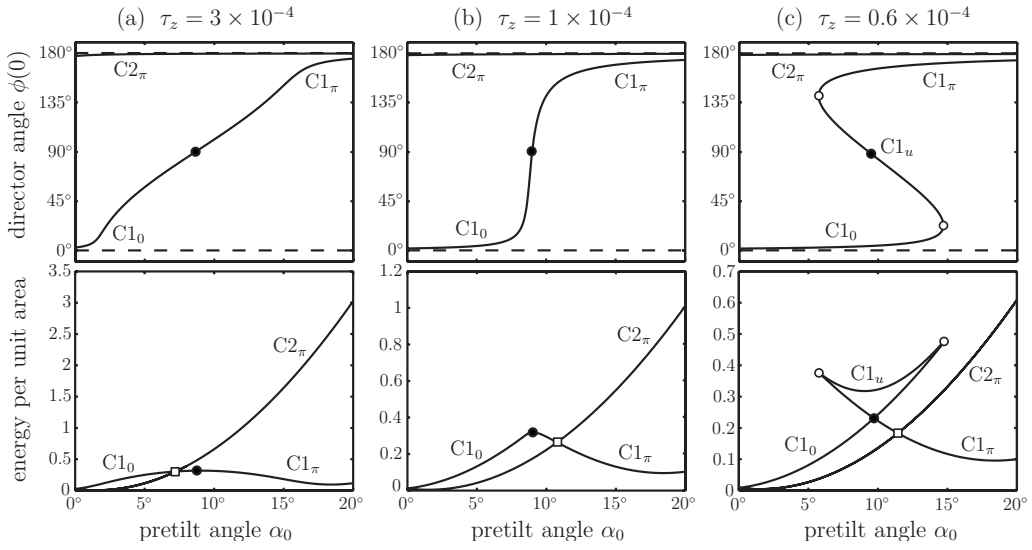

FIG. 5. The influence of variable zenithal anchoring strength on the surface director angle $\phi(0)$ (upper graphs) and the total energy per unit area (lower graphs). In (a)–(c), $\theta=10°$, $\tau_a=10^{-4}$ N m^{-1}, while τ_z is as indicated (in N m^{-1}) and $\tau_{az}=(\tau_a+\tau_z)/2$. Circles ● indicate the notional transition from $C1_\pi$ to $C1_0$ where $\phi(0)=90°$. Circles ○ signify extrema in the angle $\phi(0)$, while the squares □ correspond to energy crossover points. (The energies per unit area are in units 10^{-5} J m^{-2}.)

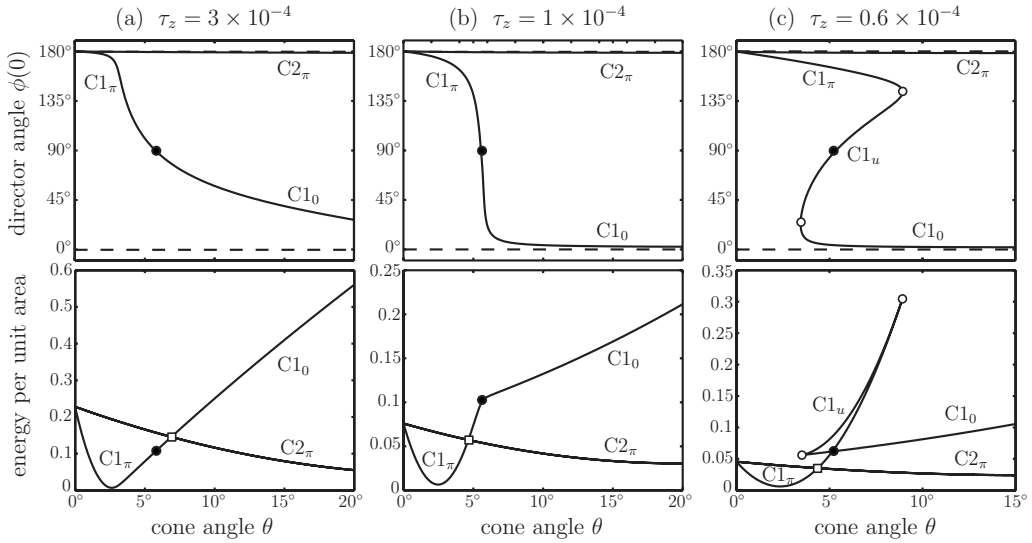

FIG. 6. The influence of variable zenithal anchoring strength on the surface director angle $\phi(0)$ (upper graphs) and the total energy per unit area (lower graphs). In (a)–(c), $\alpha_0=5°$, $\tau_a=10^{-4}$ N m^{-1}, while τ_z is as indicated (in N m^{-1}) and $\tau_{az}=(\tau_a+\tau_z)/2$. The transition and extrema indicators are equivalent to those in Fig. 5. (The energies per unit area are in units 10^{-5} J m^{-2}.)

ron configurations will exhibit different energies. It is by considering these energies that we will be able to determine the global energy minimizer of the system.

Once $\phi(0)$ and $\phi(d)$ are known, the azimuthal angle $\phi(z)$ across the bottom half of the cell in Eq. (18) can be represented using the plots presented in Fig. 4. These depict the

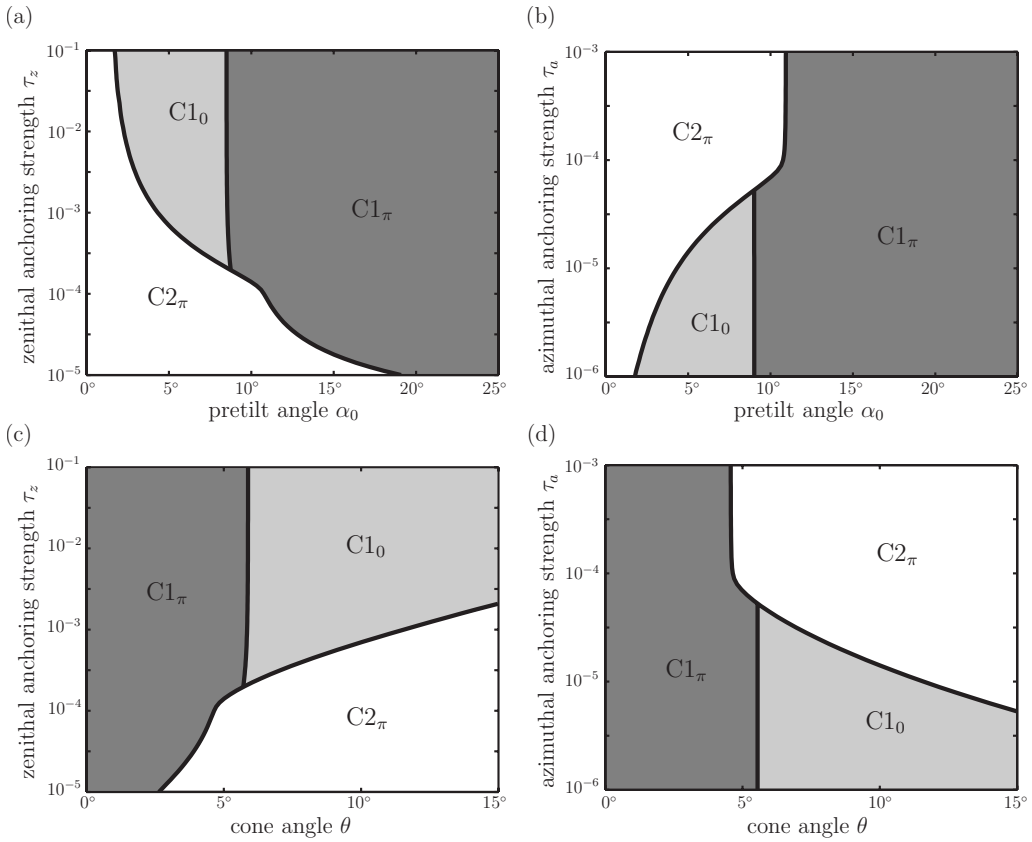

FIG. 7. Phase diagrams indicating the chevron of lowest energy as the angles or the anchoring strengths are allowed to vary. In each plot $\tau_{az}=(\tau_a+\tau_z)/2$ and anchoring strengths are in units N m^{-1}. (a) $\theta=10°$, $\tau_a=10^{-4}$ N m^{-1}; (b) $\alpha_0=5°$, $\tau_a=10^{-4}$ N m^{-1}; (c) $\theta=10°$, $\tau_z=10^{-4}$ N m^{-1}; (d) $\alpha_0=5°$, $\tau_z=10^{-4}$ N m^{-1}.

smectic cone (described in Fig. 3) as viewed along the x axis. In this plot we represent this linear variation of ϕ through the cell, from $\phi(0)$ to $\phi(d)$, using the diagrams shown in Fig. 3, and using thick solid, dashed, or dotted lines. These three different lines will denote the three possible solutions we have found: two for the C1 case and one for the C2 case. One end of these paths around the cone must be at the intersection of the C1 and C2 cones (i.e., in the xy plane) since this is the value of ϕ prescribed at $z=d$. The other ends of the paths follow either the C1 or C2 cone and end at the value $\phi(0)$ determined by the solutions of Eq. (19) with $\mu>0$ for C1 and $\mu<0$ for C2 chevrons. The two different solutions for the C1 case will be denoted by $C1_0$, for $\phi(0)$ close to 0, and $C1_\pi$, for $\phi(0)$ close to π radians. For the C2 case we only find a solution with $\phi(0)$ close to π and denote this solution by $C2_\pi$.

When both the $C1_0$ and $C1_\pi$ chevrons coexist for a given pretilt and cone angle there is a third unstable configuration with $\phi(0)$ close to $\pi/2$. Since this is an unstable solution we do not need to consider it when comparing energy values of solutions, although in the following figures we denote this third configuration by $C1_u$.

In Figs. 4–8 we have chosen the parameter values $K_\phi = 1\times10^{-11}$ N, $d=2\times10^{-6}$ m, and $\mu=0.85$. In addition, in Fig. 4 we have set $\tau_a=\tau_z=\tau_{az}=1\times10^{-4}$ N m^{-1}. When varying the azimuthal and zenithal anchoring strengths we will fix the interaction strength $\tau_{az}=(\tau_a+\tau_z)/2$. Figures 4(a)–4(e) illustrate the C1 and C2 director profiles for a fixed cone angle $\theta=10°$ and variable pretilt α_0, whereas in Figs. 4(f)–4(j) the cone angle is allowed to vary and the pretilt $\alpha_0=5°$ is constant. We find that $C2_\pi$ structures exist with $\phi(0)$ relatively close to $\phi(d)$ for each pretilt (Fig. 4). We also observe that $C1_0$ chevrons occur when the pretilt angle is small, and $C1_\pi$ chevrons when the pretilt is large relative to θ. A similar behavior is seen in Figs. 4(f)–4(j) with $C1_\pi$ chevrons prevalent when the cone angle is small. In Figs. 4(c), 4(h), and 4(i), stable $C1_0$ and $C1_\pi$ states both exist at intermediate values of the pretilt or cone angle.

In order to demonstrate the existence of the various chevron configurations, in Fig. 5 we examine the influence of variable zenithal anchoring strengths on the surface director twist angle $\phi(0)$ and the total energy per unit area E defined in Eq. (20). In each case, the pretilt angle α_0 is allowed to vary from 0° to 20°, while the cone angle is fixed at $\theta=10°$. In Fig. 5(a), when the zenithal anchoring strength is relatively strong, there is a smooth, monotonic transition from a $C1_0$ to a $C1_\pi$ dominated regime as the pretilt angle increases. In this case, at small pretilts $C2_\pi$ chevrons exhibit the lowest energy, while $C1_\pi$ configurations are the energy minimizers at large pretilts. The $C1_0$ chevrons are lowest in energy for a very small range of pretilts close to $\alpha_0=7°$. The transition from a $C1_0$ to a $C1_\pi$ chevron becomes steeper as the zenithal anchoring strength is decreased until eventually the transition is hysteretic and the two stable C1 chevrons coexist for a range of pretilt angles. Figure 5(c) illustrates this coexistence of chevrons at intermediate pretilt angles when the zenithal anchoring strength is relatively weak. For example, when $\alpha_0=10°$ it is possible to obtain four distinct values for the twist angle on the surface, $\phi(0)$, corresponding

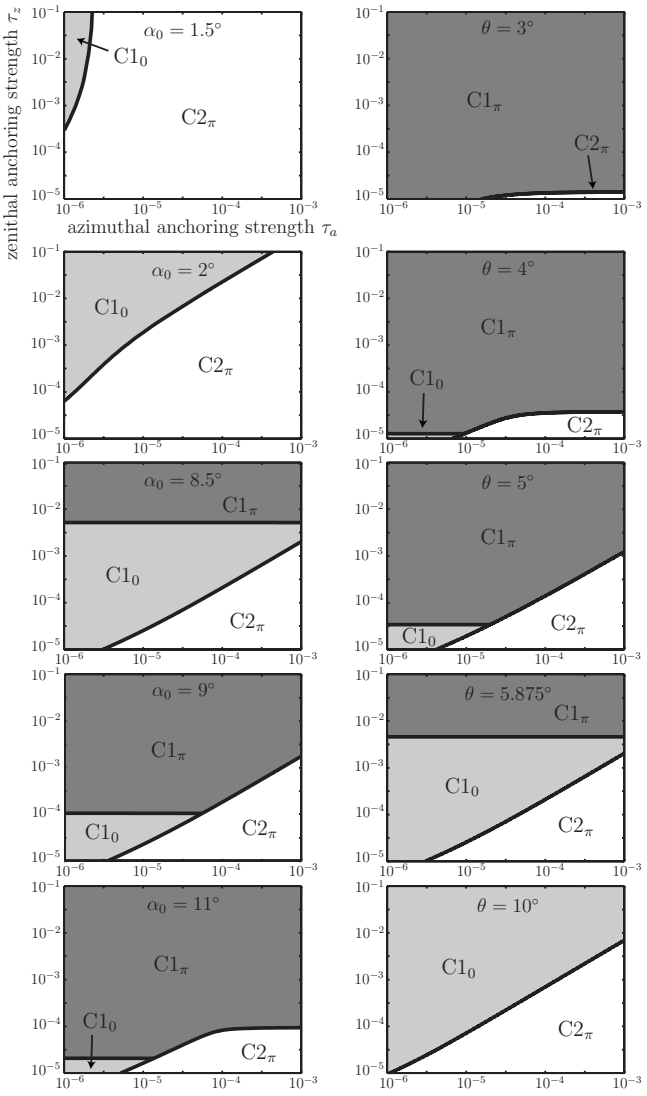

FIG. 8. Phase diagrams indicating the chevron of lowest energy as the anchoring strengths (in units N m^{-1}) are varied and for the angles indicated. In each plot the coupling anchoring also varies via $\tau_{az}=(\tau_a+\tau_z)/2$.

to $C1_0$, $C1_u$, $C1_\pi$, and $C2_\pi$ chevrons. Despite this, the energy minimizer behavior is very similar to Fig. 5(a) with $C2_\pi$ then $C1_\pi$ states dominating as α_0 increases, although the small $C1_0$ minimizing region is now absent.

Figure 6 presents an analysis similar to Fig. 5 as the cone angle θ increases, with fixed $\alpha_0=5°$. Once again, a weakening of the zenithal anchoring strength, relative to the azimuthal value, leads to a hysteresis and the introduction of unstable $C1_u$ chevrons. For small cone angles $C1_\pi$ chevrons are the energy minimizers, with a transition to $C2_\pi$ chevrons as θ increases. However, in Fig. 6(a) we note that $C1_0$ chevrons can dominate for a narrow range of cone angles, provided the zenithal anchoring is relatively strong.

Figures 5 and 6 demonstrate that the chevron configurations which minimize the total energy of the system depend upon the anchoring parameters chosen. With this in mind, in Fig. 7 we present phase diagrams that indicate the preferred chevron structures (i.e., the energy minimizer) for a range of

parameter values. These plots expand upon the results of Fig. 6 and demarcate the different chevron regimes. In Figs. 7(a) and 7(b) we see that, as the pretilt angle α_0 increases, there is a transition from $C2_\pi$ to $C1_\pi$ chevrons, which may be interspersed by an intermediate phase of $C1_0$ chevron structures when τ_z is large or τ_a is small. From Figs. 7(c) and 7(d) we see that $C1_\pi$ chevrons dominate when the cone angle θ is small. The two stage transition from $C1_\pi$ to $C2_\pi$ via $C1_0$ was illustrated in Fig. 6(a) and can be achieved by increasing the zenithal anchoring strength. Since a decrease in temperature from the Sm*A*–Sm*C* transition will be associated with an increase in cone angle θ, a horizontal line of constant anchoring strength in Fig. 7(c) or Fig. 7(d) can be interpreted as indicating the behavior as a sample is cooled. For small cone angles (high temperature) a C1 chevron is preferred, and as the cone angle increases (temperature decreasing) a C2 chevron is preferred.

Recall that the motivation for examining independent azimuthal and zenithal anchoring strengths was the apparent contradiction between the results of Wang *et al.* [17] and Diaz *et al.* [15,16]. The former finds that C2 chevrons are favored at large anchoring strengths, while the latter predict a transition from C2 to C1 chevrons as the anchoring strength increases. This apparent contradiction appears to be a consequence of the surface anchoring energies adopted in these articles. Diaz *et al.* [15,16] adopt the surface energy (2) that essentially incorporates equal zenithal and azimuthal contributions via a single anchoring strength, $\tau_z=\tau_a=\tau_{az}$. In contrast, the definition of surface anchoring employed in Wang *et al.* [17] is analogous to a purely azimuthal energy (i.e., $\tau_z \equiv 0$, $\tau_{az} \equiv 0$).

By concentrating on very small τ_z in Fig. 8, we are able to reproduce the behavior of Wang *et al.* [17]. Regardless of the pretilt and cone angles chosen, if τ_z is small then $C2_\pi$ chevrons will always dominate when the azimuthal anchoring is strong. Figure 8 is also in good agreement with Diaz *et al.* [15]. For the parameters considered, the point $\tau_a=\tau_z=10^{-5}$ N m^{-1} (corresponding to a weak unified anchoring) almost always lies within the $C2_\pi$ chevron region. As the anchoring strengths increase while maintaining $\tau_a=\tau_z=\tau_{az}$, it is possible for the system to pass into a $C1_\pi$ regime.

V. SUMMARY

We have examined the transition between C1 and C2 chevron profiles in a smectic-*C* liquid crystal cell. It is clear from the results presented here that by decoupling the azimuthal and zenithal surface energies, it is possible to ensure the existence of specific chevron structures. Strong azimuthal anchoring leads to C2 chevrons, while C1 chevrons are characteristic of relatively strong zenithal anchoring. Therefore, it is very important that any model of a smectic cell, especially a SSFLC device, should take into account the substrate treatment and the nature of the anchoring it induces. It is also possible, using the results we have presented, to deduce the behavior of a confined smectic material as the temperature is reduced from the Sm*A*-Sm*C* transition. If we fix all parameters and consider an increase in θ from zero we are, in effect, considering a reduction in temperature. For instance, if we consider the horizontal lines corresponding to parameter values $\tau_a=\tau_z=1\times10^{-4}$ N m^{-1} in Figs. 7(c) and 7(d), we see that as θ increases, the global minimum chevron state changes from $C1_\pi$ to $C2_\pi$ (while the minimum C1 state is $C1_0$). Investigation of Fig. 6 shows that, even though the $C2_\pi$ chevron has the lowest energy, the $C1_0$ state remains metastable. There may, therefore, be problems of degeneracy in the system and both chevron states may occur within the same sample, causing zigzag defects. Use of such phase diagrams to tailor the anchoring strengths will therefore be a useful guide to developing defect-free samples.

[1] T. P. Rieker, N. A. Clark, G. S. Smith, D. S. Parmar, E. B. Sirota, and C. R. Safinya, Phys. Rev. Lett. **59**, 2658 (1987).
[2] N. A. Clark and T. P. Rieker, Phys. Rev. A **37**, 1053 (1988).
[3] M. Nakagawa, Mol. Cryst. Liq. Cryst. **174**, 65 (1989).
[4] M. Nakagawa, Displays **11**, 67 (1990).
[5] S. Mukai and M. Nakagawa, J. Phys. Soc. Jpn. **62**, 1984 (1993).
[6] C. Anderson, Ph.D. thesis, University of Strathclyde, 1999.
[7] A. de Meyere, H. Paulwels, and E. de Ley, Liq. Cryst. **14**, 1269 (1993).
[8] L. Limat and J. Prost, Liq. Cryst. **13**, 101 (1993).
[9] L. Limat, J. Phys. II **5**, 803 (1995).
[10] N. J. Mottram, N. U. Islam, and S. J. Elston, Phys. Rev. E **60**, 613 (1999).
[11] N. Vaupotič, S. Kralj, M. Čopič, and T. J. Sluckin, Phys. Rev. E **54**, 3783 (1996).
[12] S. M. Beldon, N. J. Mottram, and S. J. Elston, Mol. Cryst. Liq. Cryst. Sci. Technol., Sect. A **365**, 729 (2001).
[13] A. N. Shalaginov, L. D. Hazelwood, and T. J. Sluckin, Phys. Rev. E **58**, 7455 (1998).
[14] A. N. Shalaginov, L. D. Hazelwood, and T. J. Sluckin, Phys. Rev. E **60**, 4199 (1999).
[15] A. Diaz, N. J. Mottram, and G. McKay, Eur. Phys. J. E **18**, 231 (2005).
[16] A. Diaz, N. J. Mottram, and G. McKay, Mol. Cryst. Liq. Cryst. **438**, 1581 (2005).
[17] C. Wang, R. Kurihara, P. J. Bos, and S. Kobayashi, J. Appl. Phys. **90**, 4452 (2001).
[18] A. S. Morse, H. F. Gleeson, and S. Cummings, Liq. Cryst. **23**, 531 (1997).
[19] P. G. de Gennes and J. Prost, *The Physics of Liquid Crystals* (Oxford University Press, New York, 1995).
[20] S. J. Elston and J. R. Sambles, *The Optics of Thermotropic Liquid Crystals* (Taylor and Francis, London, New York, 1998).
[21] F. Giesselmann, P. Zugenmaier, I. Dierking, S. T. Lagerwall, B. Stebler, M. Kaspar, V. Hamplova, and M. Glogarova, Phys. Rev. E **60**, 598 (1999).
[22] B. Jérôme, Rep. Prog. Phys. **54**, 391 (1991).
[23] M. Vilfan and M. Čopič, Phys. Rev. E **68**, 031704 (2003).
[24] I. W. Stewart, *The Static and Dynamic Continuum Theory of Liquid Crystals* (Taylor and Francis, London, New York, 2004).